Applied Geomatics (2026) 18:115
https://doi.org/10.1007/s12518-026-00742-x

RESEARCH

Satellite-derived bathymetry in optically complex waters: testing an SDB–KED hybrid approach in the Venice Lagoon

Federica Gerla[1,2] · **Caterina Balletti**[2]

Received: 27 February 2026 / Accepted: 14 May 2026
© The Author(s) 2026

Abstract

Accurate and up-to-date bathymetric data are essential for the management and spatial planning of transitional coastal environments, yet conventional survey methods remain costly and difficult to implement at large spatial scales and high temporal frequency. This study investigates the potential of Satellite-Derived Bathymetry (*SDB*) as a cost-effective monitoring tool, using the Venice Lagoon as a morphologically and optically complex test site. Two methodological axes were developed. The first applies a stratified log-ratio Band Ratio Method (Stumpf et al. 2003) using Sentinel-2 multitemporal imagery, calibrated against the 2002 full-lagoon bathymetric dataset (Sarretta et al. 2010), achieving a Root Mean Square Error (RMSE) of 1.09 m and an R^2 of 0.87 across the entire depth range. The second axis refines this approach through advanced radiometric pre-processing, including sun-glint correction and clean-water compositing, combined with a Random Forest substrate classification and a stratified *SDB* calibration for sandy versus muddy seafloors. The resulting *SDB* was further integrated with Kriging with External Drift (*KED*), using the 2013 CNR-ISMAR (National Research Council Institute of Marine Sciences) multibeam survey as ground truth. This hybrid *SDB-KED* model achieved an R^2 of 0.73, an RMSE of 2.55 m, and a near-zero bias (-0.09 m) over more than 320,000 validation points, demonstrating effective bathymetric reconstruction across the full lagoon depth range. Residual uncertainties are concentrated at channel margins and in areas exceeding 15 m depth, where optical signal extinction limits satellite penetration. The proposed framework, implemented entirely on open-source data and cloud computing platforms, offers a replicable and scalable protocol for supporting spatial planning in dynamic coastal and marine environments.

Keywords Satellite-derived bathymetry (SDB) · Sentinel-2 · Multispectral remote sensing · Coastal and maritime spatial planning · Venice lagoon · Kriging with external drift

Introduction

The transition areas between the terrestrial and marine domains are critical ecotones where physical, biological and socio-economic variables converge and overlap, creating an environmental balance that is as sophisticated as it is precarious (Elliott et al. 2007; Tagliapietra et al. 2014). Precisely because of this multidimensionality, the *Land-Sea Interactions* (LSI) paradigm[1] has established itself as the theoretical and operational centre of gravity for decoding and addressing the dynamics of co-evolution between land and sea, finding formal legitimacy in the European framework for maritime spatial planning (European Commission 2014).

The need to translate this paradigm into effective governance strategies is made urgent by the increased

✉ Federica Gerla
federica.gerla@uniroma1.it; fgerla@iuav.it

Caterina Balletti
balletti@iuav.it

[1] National PhD in Earth Observation, Department of Civil and Environmental Engineering (DICEA), Sapienza Università di Roma, Roma 00185, Italy

[2] CIRCE Laboratory of Cartography and GIS, Department of Architecture and Arts, Università Iuav di Venezia, Dorsoduro 1827, 30123 Venezia, Italy

[1] The term *Land-Sea Interaction* refers to the complex system of interdependencies between natural processes and human activities that connect the mainland and the sea. This concept requires integrated management of the coastal zone, going beyond the shoreline as an administrative boundary to consider it a dynamic transition zone (Creamer et al. 2020).

Published online: 20 June 2026

anthropogenic pressure on coastal areas. The growing concentration of population and activity, with around 40% of the planet's inhabitants living within 100 km of the coastline, acts as a catalyst for the degradation of these ecosystems, requiring the systematic integration of LSIs into land management policies (Innocenti and Musco 2023; O'Hagan et al. 2020; Schlüter et al. 2020). This picture of anthropogenic vulnerability is compounded by forces deriving from climate change, which acts as a multiplier of critical issues (IPCC 2022; ISPRA 2023), triggering sudden morphological transformations that threaten the stability of these territories. Coastal planning and maritime spatial planning are therefore called upon to move beyond a purely two-dimensional and 'flat' view of the territory. It is therefore essential to incorporate the vertical dimension into decision-making processes: analytical knowledge of the depths and morphology of the seabed is no longer an ancillary technical data, but an integral and structural part of land protection choices (Iglesias-Campos et al. 2021). Traditional bathymetric surveying methods, from single-beam and multi-beam echo sounders to bathymetric LIDAR surveys (Fernandez-Diaz et al. 2013) or UAV platforms (Agrafiotis et al. 2019; Karaki et al. 2022), guarantee high accuracy but are costly and time-consuming to acquire, especially in large and morphologically complex environments (Lurton et al. 2015; Francis and Traykovski 2021; Del Savio et al. 2023; Ferreira et al. 2022; Ferrando et al. 2021). This limits their systematic applicability on a large scale and makes it difficult to implement high-frequency monitoring programmes, despite the fact that legislation and planning tools on the subject effectively push for continuous updating of the seabed as a necessary condition for authorising and evaluating any management, protection or adaptation intervention[2] (Campa 2007; Torelli 2020).

In response to these limitations, there is growing scientific and practical interest in Earth observation applications aimed at satellite-derived bathymetry (*SDB*) based on the processing of multispectral images (Gao 2009; Hedley et al. 2012). *SDB* allows depth estimates to be made over large areas, with higher update frequencies and significantly lower costs than conventional techniques, making it particularly promising for monitoring shallow coastal-marine and lagoon environments (Stumpf et al. 2003; Mahrad et al. 2020; Caballero and Stumpf 2019; Ashphaq et al. 2021; Hodúl et al. 2018; Figliomeni and Parente 2023; Ahola et al. 2020; Kader et al. 2013).

In light of these premises, the present research aims to test *SDB* models within the Venice Lagoon basin, using this context as a testing ground, precisely because of the complexity that characterises the area.

Although the Venice Lagoon is an area of great importance and interest, it suffers from a lack of up-to-date bathymetric data: the most recent comprehensive open-data maps date back to 2002 (Sarretta et al. 2010), while the most recent survey (from 2013), although highly accurate, is spatially confined to tidal channels and port mouths (Madricardo et al. 2017a, b). The work therefore uses both datasets as *ground truth* bases, employing them not only for model calibration but also as terms of comparison for a critical assessment of the morphological changes that have occurred.

The research architecture is structured according to a dual methodological perspective, continuing and further developing a line of investigation aimed at validating the robustness of satellite data in optically complex scenarios. The first axis, which is applicative and demonstrative in nature, implements an operational procedure in Google Earth Engine based on the Band Ratio Method (Stumpf et al. 2003). The objective is to generate continuous bathymetric mapping from Sentinel-2 images, optimising the signal response in the first few metres of water through stratified calibration by depth classes. To validate this first test, the results are compared with the aforementioned 2002 reference dataset, allowing the accuracy of the estimate to be quantified and the validity of the satellite data to be confirmed.

The second axis of the research evolves towards an analytical study aimed at testing the robustness of other *SDB* models in conditions of high heterogeneity and turbidity. The workflow, this time developed in Google Earth Engine and Google Colab, integrates advanced pre-processing of Sentinel-2 images and adopts stratified calibration by sediment class. This 'dual-track' approach overcomes the limitations of global models by assigning calibration parameters specific to the nature of the substrate to improve the stability of the estimate. The validation of this second test uses the CNR-ISMAR (2013) multibeam survey[3] (Madricardo et al. 2017a). Finally, the work continues with testing the integration of Kriging with External Drift (*KED*) (Chiles and Delfiner 2012; Xu et al. 2022) to *the SDB* derived from the stratified Band Ratio Method: satellite spectral information is used as an auxiliary variable (drift) to spatially extend point surveys. This geostatistical integration allows local errors to be corrected and a continuous and physically

[2] See Legislative Decree 152/2006 (Environmental Regulations), which defines the knowledge frameworks necessary for soil and water protection; Legislative Decree 201/2016 (Maritime Spatial Planning) and Legislative Decree 190/2010 (Marine Strategy), which make the effectiveness of management and adaptation plans dependent on the accuracy and constant updating of bathymetric and morphological data.

[3] The 2013 multibeam survey was produced by CNR-ISMAR (Institute of Marine Sciences) using the Kongsberg EM-2040 system, ensuring a spatial resolution of 0.5 m focused on the network of main channels.

consistent bathymetric surface to be reconstructed, even in deep channels where the optical signal alone is insufficient.

The results of the two operational phases will be analysed comparatively to determine the best-performing model in the study area and to outline the methodological limitations encountered.

Description of the study area

The Venice Lagoon (Fig. 1) is the largest coastal transition system in the Mediterranean, covering an area of approximately 550, km^2 s with a longitudinal development of 50 km (Campa 2007).

The hydrodynamic and geomorphological structure of the basin is governed by the three port mouths, Lido, Malamocco and Chioggia, which regulate water exchange with the Adriatic Sea, dividing the lagoon into three sub-basins with different residence times and exchange dynamics (Ravera 2000; Campa 2007). The morphology is characterised by a clear prevalence of submerged or intertidal environments: only 8% of the surface area consists of emerged areas, while the remainder is divided into a complex network of port and tidal channels, mudflats and vegetated salt marshes (D'Alpaos 2011).

From a bathymetric point of view, the basin has a marked bimodality, alternating between navigation channels up to 20 m deep and intertidal areas generally less than 5 m deep, furrowed by a dense network of ghebi (ibid.). This morphological heterogeneity is reflected in the distribution of sediments, which vary from coarse sand near the inlets to silty-clay deposits in the innermost areas (Ravera 2000). The optical properties of the water column are influenced by the hydro-sedimentary articulation, presenting increasing turbidity gradients towards the interior (Gianinetto and Lechi 2004). The penetration of light radiation is conditioned by the concentration of suspended particles and the nature of the seabed, defining an optically complex domain. Added to this complexity is a structural sediment deficit, estimated at approximately 1.1×10^6 m³ year^{-1}, which determines a progressive deepening of the seabed and the consequent loss of intertidal habitats (Campa 2007; Toso 2017).

Finally, the recent evolution of the system is influenced by the combined action of eustasy and subsidence, which have produced a relative sea level rise of approximately 23 cm over the last century (Gatto and Carbognin 1981). These forcing factors not only increase the vulnerability of the basin to high water events but also alter hydrodynamic processes and overall morphological stability.

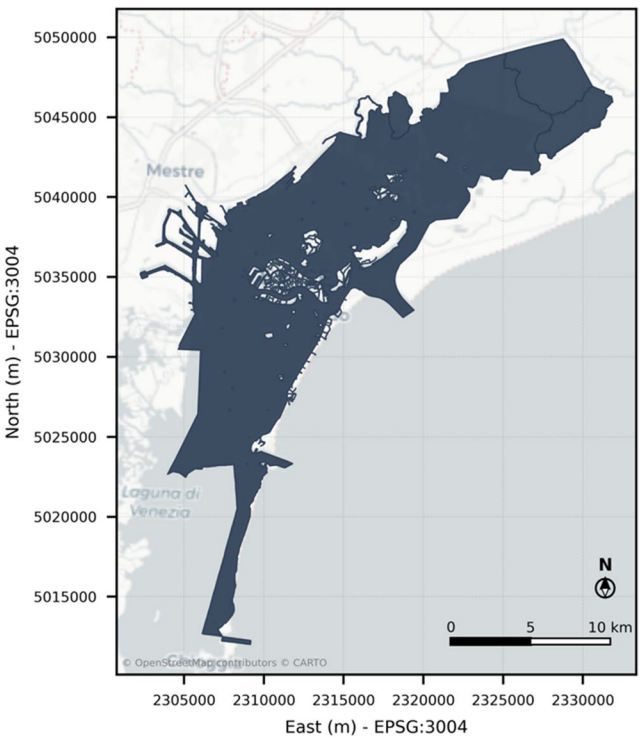


Fig. 1 Representation of the test area of the Venice Lagoon basin (EPSG reference system: 3004)

Methodology

The methodology adopts a two-axis approach (Table 1): an initial large-scale analysis and a subsequent level of metric detail on the same area, resulting from a workflow optimisation process aimed at overcoming the limitations identified in the preliminary phase.

The first axis aims to validate a satellite-derived bathymetry (*SDB*) model using a multi-temporal and stratified approach. The procedure integrates the selection and preprocessing of Sentinel-2 images with a regressive modelling phase for depth classes, in order to test the sensitivity of the optical signal with respect to integral bathymetric datasets and evaluate the metric accuracy achievable in complex lagoon environments.

The axis develops through a sequence of operational phases that guide the entire bathymetric estimation process: from the acquisition and pre-processing of satellite images, to the calculation of the pseudo-bathymetric index (*pSDB*), to stratified sampling by depth classes. The latter forms the basis for calibrated regression modelling for each bathymetric band, the results of which are applied to generate the final segmented raster, representative of the estimated bathymetry of the study area. The quality of the product obtained is finally assessed through a validation phase, conducted by comparison with the 2002 reference bathymetric data (Table 2).

Table 1 Methodology workflow, divided into Axis 1 and Axis 2

Work phase	Axis 1	Axis 2
Data acquisition	Acquisition of harmonised Sentinel-2 L2A images (BOA + SCL)	
Time selection	1–7 April 2020	March 2020 - June 2020
Masking filters	Cloud filter < 10% and multi-index masking (*NDVI*, *NDWI*, *MNDWI*, *AWEI*, *AWEIsh*, *NDWI_L*)	Cloud filter < 10%, *SCL* mask (removal of unsuitable classes) and combined water mask (*SCL* + *NDWI*/*MNDWI* + *NDVI* threshold)
Radiometric pre-processing	—	Sun-glint correction (Hedley et al. 2005) applied to visible bands and calculation of multi-temporal composite based on the 25th percentile of reflectance
Optical composite	Multi-temporal average of *pSDB* on the entire image series (Stumpf et al. 2003)	Multi-temporal 'clean-water' composite (25th percentile) on optical bands
Ground truth (GT)	Lagoon Bathymetry Cigno 2002 (Sarretta et al. 2010)	MBES Survey 2013 (CNR-ISMAR 2013, RITMARE)
Bathymetric index calculation	Calculation of blue/green *log-ratio* index for pseudo-bathymetry (Stumpf et al. 2003)	Calculation of blue/green *log-ratio* index (Stumpf et al. 2003)
Sampling for calibration	Stratified sampling by depth (5 classes)	Random sampling of 10,000 pixels distributed across the entire bathymetric range
SDB model calibration	Linear regressions for the 5 bathymetric classes	Global linear regression and subsequent stratified calibration by substrate type (sand vs. mud)
SDB production	Generation of continuous bathymetric map from stratified models	Calibrated SDB production and residual map calculation
Model validation	Pixel-by-pixel difference, regression on random sample (1000 points) and calculation of *RMSE*, *MAE*, R^2, and average *bias*	Statistical validation on GT CNR_ISMAR 2013 dataset and calculation of *RMSE*, *MAE*, R^2, and average *bias*
Stratification by substrate	—	Seabed classification (Random Forest: Sand vs. Mud) and *SDB* calibration with separate regressions for each substrate type
Geostatistical integration	—	*SDB* integration with kriging with external drift (*KED*)
Final output	Continuous bathymetric map derived from stratified *SDB*	Final *SDB-KED* integrated bathymetric map with 10-metre spatial resolution

Table 2 Technical characteristics of the 2002 dataset used as ground truth

Technical item	Description
Year of acquisition	2002
Responsible body	Venice Water Authority (now Venice Lagoon Authority)
Survey technology	Multibeam for the main channels (depth > 5 m) and the three lagoon inlets Single-beam echo sounder for shallow waters and secondary channels (< 5 m) Traditional topographic method (stadia rod + GPS) for very shallow areas near the salt marshes Stereo aerial photogrammetry for the distribution of salt marshes
Spatial resolution	10 m
Coverage	Entire Venice Lagoon (approximately 409 km²)
Vertical reference (Datum)	IGM42 (mean sea level, Genoa 1942)

The second axis of research is dedicated to the evaluation of a set of progressive strategies and methodological refinements for modelling lagoon bathymetry. In this phase, the work evolves by introducing spectral refinement procedures which, through sun-glint correction (Hedley et al. 2005) and the creation of multi-temporal 'clean-water' composites, allow the seabed signal to be isolated more accurately from disturbances caused by residual turbidity. At the same time, to manage the heterogeneity of the basin, a substrate stratification strategy based on the Random Forest algorithm is implemented: this classification separates sandy seabeds from muddy ones, allowing differentiated calibrations to be applied that take into account the different reflective response of the sediments. The final methodological aspect tested by this second strand is the hybrid integration of remote sensing and geostatistics through the application of Kriging with External Drift (*KED*). This geostatistical method allows the combination of a deterministic component, derived from external explanatory variables, with a stochastic component that models the spatial autocorrelation of the residuals (Goovaerts 1997; Chiles and Delfiner 2012; Monteys et al. 2015; Casal et al. 2019, 2020). The second axis does not represent a direct methodological alternative to the first, but rather an integrated and optimised workflow in which radiometric refinement, substrate stratification and geostatistical integration are combined to address the optical and morphological l complexity of the lagoon environment. Again, there is a comparison with Ground Truth data from 2013 provided by CNR-ISMAR (Table 3).

Table 3 Technical characteristics of the 2013 dataset used as ground truth

Technical item	Description
Year of acquisition	May - December 2013
Responsible body	CNR-ISMAR (RITMARE Project) and Hydrographic Institute of the Navy (IIM)
Survey technology	Kongsberg EM-2040 (dual-head) 360 kHz multibeam echo sounder (MBES)
Spatial resolution	0.5 m (Digital Terrain Model)
Coverage	2,500 linear kilometres of tidal channels and harbour mouths in the Venice Lagoon (partial coverage: does not include salt marshes and mudflats)
Vertical reference (datum)	Punta Salute 1897 (NANZ)
Tidal correction method	3D SHYFEM hydrodynamic model with data assimilation from 93 virtual stations

Axis I: *SDB* modelling and stratified validation through comparison with the 2002 dataset

Acquisition and pre-processing of satellite images

The initial phase of the work involved the retrieval and selection of satellite data. Specifically, Sentinel-2 images were acquired from the Copernicus Level-2 A collection, which provides multispectral (MSI) products with spatial resolution up to 10 m and a high revisit frequency (2–3 days at mid-latitudes). To ensure the necessary radiometric consistency in multi-temporal analyses, the harmonised version of the dataset was adopted. In this case, the products have already undergone atmospheric correction using the Sen2Cor (Bottom-of-Atmosphere reflectance) algorithm, including the scene classification layer (SCL), which is essential for optimising masks and identifying suitable pixels. The analysis was limited to a time interval between 1 April 2020 and 7 April 2020. The selection of this time window was motivated by the measures taken to contain the COVID-19 pandemic, which led to a drastic reduction in lagoon traffic. This scenario offers the opportunity to analyse the system's response under conditions of minimal anthropogenic disturbance, assuming a consequent attenuation of turbidity linked to the resuspension of sediments induced by the wave motion of vessels. This interval was chosen with the intention of favouring favourable lighting conditions and limiting the frequency of extreme events that can alter the optical properties of the water column.

To ensure the radiometric quality of the selected images, a cloud cover filter was applied, excluding all scenes with a cloud pixel percentage greater than 10%. This threshold was selected as a compromise between temporal availability and data quality, while avoiding overcast conditions that would compromise the passage of radiation through the aquatic medium. A series of spectral transformations were applied to each image to improve the discrimination between aquatic and non-aquatic surfaces. In particular, the following indices were calculated and the relative thresholds for masking were defined (Table 4). The selection of the indices and threshold values adopted is based on an analysis of the relevant scientific literature, in which these parameters are widely used and validated for lagoon and coastal contexts.

Table 4 Indices and relative thresholds adopted for masking

Index	Description	Values for masking	Source
NDVI	Normalised Difference Vegetation Index	NDVI < -0.2	Sentinel Hub, 2021
NDWI	Normalised Difference Water Index	NDWI > 0.4	McFeeters 1996
MNDWI	Modified Normalised Difference Water Index	MNDWI > 0.42	Xu 2006
AWEIsh	Automated Water Extraction Index shadow	AWEIsh > 0.1112	Feyisa et al. 2014
AWEInsh	Automated Water Extraction Index non-shadow	AWEInsh > 0.1879	Feyisa et al. 2014
NDWI_L	Normalised Difference Water Index using bands B8 and B11	NDWI_L > 1	Sentinel Hub, 2021

Calculation of the pseudo-bathymetric index (*pSDB*)

Once the image filtering and masking phase was complete, each scene was subjected to the calculation of a derived spectral indicator, called *logRatio*, commonly used in the literature for bathymetric estimation in shallow environments (Stumpf et al. 2003; Lyzenga 1978). This index is based on the principle that the selective absorption of light by the water column is a function of wavelength: blue radiation (B2) penetrates deeper than green (B3) or red (B4), and the logarithmic ratio between these bands can therefore be related to depth. The *logRatio* was calculated as follows:

$$logRatio = log\left(\frac{B2}{B_x} \bullet \ nConst\right) \quad (1)$$

where B2 represents the reflectance in the blue band, while Bx is the dynamically selected denominator: the green band (B3) or red band (B4) will be selected depending on the depth of the test area. In this study, the green band was considered, which, having a wavelength of ~ 560 nm, is suitable for estimates in shallow/intermediate waters, such as the Venice Lagoon (Stumpf et al. 2003). The ratio, normalised by a constant (*nConst*), takes on a distinct function depending on the stage of processing. In the exploratory phase, the value is multiplied by a scale factor (*mp*) to generate pseudo-bathymetry (*pSDB*): a relative, uncalibrated estimate that

describes the preliminary morphological trend. In the final modelling phase, however, the *logRatio* is used directly as an independent variable in linear regression models. At this stage of the work, the output consists of a raster image in which each pixel reports the average *pSDB* value derived from the entire selected time series, serving as the basis for subsequent calibration with real data.

Stratified sampling by class

The average *pSDB* image is combined with a validated and appropriately aligned bathymetric raster, so that both the remotely estimated value (*pSDB*) and the actual depth measured in situ are available simultaneously for each spatial position. This combination forms the basis for the subsequent sampling and calibration phase. The dataset is constructed using a dedicated function that filters pixels based on predefined bathymetric thresholds corresponding to specific depth classes. A logical mask is applied to each interval and up to 200 samples are selected at random. Each point is associated with a numerical identifier (class) representing the bathymetric range to which it belongs.

The five bathymetric classes defined, consistent with the lagoon morphology, are described in Table 5 below.

These five collections are then merged into *a* single *FeatureCollection*, which represents the stratified sampling of the entire bathymetric range. Each feature contains the spatial coordinates, the average *pSDB* value (which is not yet expressed in metres), the associated actual depth and the class code. This procedure ensures the representativeness of the entire bathymetric range, allowing for stratified calibration that takes into account spectral variations as a function of depth. The extracted dataset forms the basis for model calibration.

Regressive modelling for bathymetric classes

Once the stratified sampling phase is complete, the regression models are calibrated. The aim of this operation is to quantify the relationship between the pseudo-bathymetry values (*pSDB*), derived from Sentinel-2 images, and the actual bathymetry values from the reference model. A script has been developed that allows a separate linear regression to be estimated for each of the five bathymetric depth classes previously defined during the segmentation phase. For each group, the *pSDB* values are related to the actual bathymetry through a linear function as described below:

Table 5 Depth classes defined for stratified sampling

Depth class	Depth range
Class 1	0 to -1 m
Class 2	from −1 to -2 m
Class 3	from −2 to -4 m
Class 4	from −4 to -6 m
Class 5	from −6 to -18 m

$$SDB_{finale} = m_1 \bullet pSDB + m_0 \quad (2)$$

where the coefficient *m1* represents the slope of the regression line, i.e. how much the actual bathymetry varies for a unit variation in *pSDB*. The term *m0* is the intercept, the value of the estimated bathymetry when *pSDB* is zero: it represents a reference value that determines the 'vertical shift' of the line. Each model is associated with a coefficient of determination R^2, which quantifies the proportion of the variability of the actual bathymetry that is explained by *the pSDB*. An R^2 value close to 1 indicates a high predictive capacity of the model, while lower values indicate greater dispersion and therefore lower accuracy. These intermediate results allow us to compare the performance of the models between classes and to evaluate how the pSDB-bathymetry spectral relationship varies with depth.

In parallel with segmented calibration, a global modelling phase was implemented that does not rely on bathymetric class division. At this stage, the entire set of samples is subjected to a single linear regression, applied to the entire extent of the lagoon. This approach allows the average coefficients *m1* (slope) and *m0* (intercept) to be extracted for the entire study area, serving as a benchmark. The generation of a global bathymetric map calculated using these parameters allows us to assess, during the validation phase, whether the adoption of a simplified model is able to correctly describe the lagoon morphology or whether, on the contrary, the optical variability of the seabed necessarily requires a stratified approach to contain the root mean square error (RMSE).

Generation of the final segmented raster

The outcome of the procedure is a set of stratified linear models, each calibrated to a specific bathymetric range, whose coefficients are reinserted into the workflow in Google Earth Engine to produce the final estimated bathymetry raster. This integration allows the spectral relationships detected to be translated into a continuous depth map, calibrated and consistent with the reference data.

Validation by comparison with reference bathymetric data

To assess the quality of the estimated result, a quantitative comparison was made between the bathymetric raster obtained from satellite (SDB_{finale}) and the 2002 GT reference bathymetric model.

A pixel-by-pixel difference is performed between the bathymetry value estimated by satellite and the actual value. The result of this operation is a difference raster in which

each pixel represents the local deviation between the estimate and the observation. To summarise the accuracy of the model, the script calculates various descriptive statistics on the distribution of errors.

A further comparison is performed using a random sample of 1,000 points distributed over the test area. For each point, the estimated and observed values are recorded, generating a table containing pairs of values used to compare the two models and estimate the degree of reliability of the satellite-derived bathymetry. Again, a linear regression is applied between the estimated and observed values to obtain a comparison between estimated and actual bathymetry.

Axis 2: Substrate characterisation and *SDB-KED* integration and stratified validation by comparison with the CNR-ISMAR 2013 dataset

Acquisition and pre-processing of satellite images

At this stage, the time frame was extended to the period March-June 2020. This choice reiterates the strategy of operating under conditions of minimal anthropogenic disturbance (COVID-19 restrictions), while favouring optimal lighting conditions and reduced turbidity induced by water traffic, factors that are essential for the stability of the optical properties of the water column. A restrictive atmospheric quality criterion was added to this selection, requiring cloud cover to be less than 10%. In this case, too, masking was applied, but more finely than in Axis 1, based on the Scene Classification Layer (SCL) with the aim of excluding pixels associated with classes unsuitable for water analysis. In particular, pixels with SCL equal to 0 (No Data), 1 (Saturated/Defective), 3 (Cloud Shadows), 8 (Cloud medium probability), 9 (Cloud high probability), 10 (Thin cirrus) and 11 (Snow or ice) were removed. The resulting mask therefore retains the classes deemed suitable for processing, significantly reducing contamination from clouds and shadows, which in a lagoon environment can be particularly problematic due to the high fragmentation of the landscape and the presence of mixed surfaces.

A further step involves the correction of sunglint using the approach of Hedley et al. (2005). The procedure uses the near-infrared band B8 (NIR) as a proxy for the specular component due to the water surface and applies the correction to the visible bands B2 (blue), B3 (green) and B4 (red). The corrective term is estimated only on water pixels, selected using a preliminary mask based on the Normalised Difference Water Index (NDWI), imposing the threshold NDWI > 0.3. Within this mask, the minimum NIR (B8) value is calculated for the area of interest and used as a reference (nirMin) to avoid overcorrection and make the subtraction of the specular component more robust. The correction is then performed by subtracting, for each visible band, a term proportional to (NIR – nirMin), where the proportionality coefficient is obtained by linear regression between NIR and the band considered, always calculated on water pixels. This choice is aimed at reducing radiometric artefacts related to surface ripples and specular reflection, which alter the observed reflectance without relation to depth.

After the masking and glint correction phase, the entire pre-processed collection is synthesised into a clean-water multi-temporal composite using a percentile reducer, adopting the 25th percentile. This choice implies that, for each pixel and for each band, a relatively low radiometric value is selected compared to the temporal distribution observed in the period considered. The underlying assumption is that lower reflectance values in the visible bands, with the same geometry and masking, are often associated with conditions of lower turbidity and less surface disturbance. The composite includes bands B2, B3, B4, B8, B11, B12 and SCL itself. Three spectral indices are then calculated on the 25th percentile composite and used to construct a more robust water mask: Normalised Difference Vegetation Index (NDVI), Normalised Difference Water Index (NDWI) and Modified Normalised Difference Water Index (MNDWI). The final water mask therefore combines several criteria, with the aim of reducing false positives and including only pixels that are actually submerged and suitable for *SDB*. In particular, the pixel must be classified as water by the SCL (SCL = 6) and must satisfy at least one of the two spectral conditions: NDWI > 0.3 or MNDWI > 0.2. At the same time, in order to reduce contamination due to emerged or densely submerged vegetation (vegetated sandbanks, grasslands, macroalgae), an additional constraint of NDVI < 0.1 is imposed. The resulting mask is finally applied in order to retain only those pixels that fully satisfy all the defined selection criteria. It should be noted that the mask has been defined using conservative criteria in order to exclude emerged surfaces and vegetation, while ensuring the spatial continuity of the optical predictor necessary for subsequent geostatistical integration using *KED*. The final exported dataset includes glint-corrected spectral bands in the visible and near-infrared (B2, B3, B4, B8), together with spectral indices (NDVI, NDWI, MNDWI) calculated on the composite, masked for aquatic areas only.

Calibration of the *SDB* model and generation of 10 m bathymetry

In line with the output of the pre-processing phase, the *SDB* procedure was implemented with a metric resolution of 10 m. This processing represents the reference model for the entire methodological axis, providing an initial continuous estimate of depth derived solely from radiometric

information. This product serves as a comparative baseline, allowing for explicit quantification of the improvement introduced by the subsequent phases of substrate stratification and geostatistical integration using *KED*. As already described in axis 1, the methodology adopted is based on the log-ratio approach of Stumpf et al. (2003). In this case, a high-resolution bathymetry dataset acquired as part of hydrographic surveys conducted in the network of canals in the Venice Lagoon and produced by the Institute of Marine Sciences of the National Research Council (CNR-ISMAR) was used for the calibration and validation of *the SDB*. The data consists of a bathymetric grid in raster format (ASCII ESRI), with a spatial resolution of 0.5 m, and represents a Digital Terrain Model (DTM) of the lagoon seabed limited to the areas covered by the survey.

The multiple layers were aggregated by calculating the pixel-wise average, obtaining a single, continuous bathymetric raster, cropped to the test area. The use of a multi-raster average follows a logic similar to that adopted in the clean-water composite: just as the 25th percentile on Sentinel-2 images aims to select 'favourable' radiometric conditions, reducing episodic contamination in the form of turbidity and residual surface disturbances, in the same way, the average of multiple bathymetric products allows for the attenuation of noise and non-systematic discontinuities, producing a more stable reference for the estimation of model parameters.

From the Sentinel-2 composite obtained at the end of the pre-processing phase, bands B2 (blue) and B3 (green) were selected, which constitute the information core of the *SDB* model adopted. The extraction of these bands was accompanied by a new application of the final waterMask, so as to explicitly constrain the calculation domain to only those pixels which, based on the consistent combination of SCL (Scene Classification Layer) classification, spectral indices (NDWI and MNDWI) and additional constraint on the NDVI, are effectively submerged and free from contamination attributable to emerged surfaces or significant vegetation cover. In this way, the bathymetric predictor is constructed exclusively on radiometric conditions compatible with the physical assumptions of the model.

Once the cartographic product of the logarithmic reflectance ratio (log-ratio) was obtained, the depth estimate required local calibration. At this stage, the calibration was set to cover the entire bathymetric range compatible with the spectral response of lagoon waters, aiming to maximise the investigation domain without imposing preliminary restrictive thresholds. This choice made it possible to include both the wide tidal flats and the deepest channel sections in the model, where the optical signal maintains a correlation with the seabed. Within this domain, 10,000 pixels were sampled, associating each sample with both the spectral ratio value and the reference depth.

The relationship between the logarithmic ratio and depth was then estimated using linear regression, applying the coefficients derived from the Stumpf et al. (2003) model already described in Axis 1 and ensuring the stability of the calculation by processing zero or negative reflectance values. The estimated coefficients were then applied to the entire reflectance ratio layer (previously masked on water surfaces), producing a preliminary deterministic bathymetric estimate.

The result is a continuous 10 m bathymetric model, consistent with the resolution of the optical bands used.

Substrate characterisation: Random forest classification of seabed optical classes

The classification of the lagoon seabed was carried out using a supervised approach based on the Random Forest algorithm, with the aim of discriminating between two functional sedimentological macro-types: sandy seabeds ( ) and fine-grained seabeds (Mud). This methodological choice stems from a joint assessment of the characteristics of the available sedimentological data and the intrinsic physical limitations of optical observation in a lagoon environment, where the spectral separability of the granulometric classes is strongly influenced by three factors: water column, turbidity and reduced average depth.

In this case, the ground truth data is represented by a raster of the grain size distribution of the surface sediments of the lagoon seabed, produced by the Interregional Superintendency for Public Works (1997–1998) and based on Shepard's grain size classification. The original dataset distinguishes five sedimentological classes: sand, silty sand, sandy silt, silt and clayey silt. Preliminary analysis of the class histogram shows a distribution that is heavily biased towards fine sediments: the sandy class represents a minority portion of the dataset, while the fine-grained classes are clearly dominant. This asymmetry reflects the predominantly fine nature of the Venetian lagoon seabed and has direct implications for the classification strategy adopted. The five original classes were therefore reclassified into two functional macro-classes: Sand (comprising only the 'sand' class, coded with a value of 1) and Mud (comprising all the remaining classes of silty sand, sandy silt, silt and clayey silt, reclassified with a value of 2). The binary ground truth raster was further masked using the water mask derived from the Sentinel-2 composite, ensuring that the classification process was limited exclusively to submerged pixels that were directly comparable with the optical predictors. The spectral bands B2 (Blue), B3 (Green), B4 (Red)

and B8 (NIR) were used for prediction, supplemented by the spectral indices NDWI and MNDWI. In this case, the NDVI index was deliberately excluded from the final set of predictors, as it is not very informative in submerged environments and is a potential source of radiometric noise, especially in the presence of aquatic vegetation or very low water conditions.

The training dataset was generated using stratified sampling, imposing a balanced number of samples for each class (500 for sand and 500 for mud) in order to mitigate the effect of the intrinsic imbalance of the reference data and improve the classifier's discriminatory capacity.

The Random Forest classifier was trained using a configuration of 200 decision trees, a parameter optimised to balance computational efficiency with robust generalisation capacity, avoiding overfitting phenomena. The performance analysis obtained during testing shows the following results: overall accuracy stands at 94.2%, supported by a Kappa statistical index of 0.8. It should be noted that these values reflect only the model's ability to distinguish between the two sub s from a radiometric point of view. This distinction, however clear, does not resolve the intrinsic critical issues of bathymetric estimation, such as optical signal saturation or the influence of residual turbidity, factors that affect data quality regardless of the sedimentological nature of the seabed.

The asymmetries found, with fine seabeds erroneously identified as sandy, derive from the high reflectance in shallow waters that saturates the optical signal. This is a known limitation in the literature on passive remote sensing in lagoon environments (Lyzenga et al. 2006; Misra et al. 2018). The trained classifier was finally applied to the entire lagoon area, still constrained by the water mask, producing a binary map of the seabed (Sand vs. Mud) with a spatial resolution of 10 m.

The binary map thus obtained made it possible to verify whether the nature of the substrate systematically influenced the accuracy of the bathymetry estimated with the Stumpf algorithm. It was decided to evolve the estimation procedure towards a stratified approach. Instead of a single regression for the entire lagoon, two distinct local functions were calibrated: one specific for areas identified by the model as sandy and one for those classified as fine-grained.

$$SDB_{final} = \begin{cases} m_{1,sand} + m_{0,sand} & se\ Class = Sand \\ m_{1,mud} + m_{0,mud} & se\ Class = Mud \end{cases} \quad (3)$$

This hybrid model allows the depth-reflectance relationship to be adapted to the specific optical properties of the benthos, correcting for drifts on fine sediments and ensuring a more consistent and accurate bathymetric reconstruction of the entire basin.

Optimisation of stratified SDB data using Kriging with external drift (KED) geostatistical integration

Although the log-ratio model of Stumpf et al. (2003) is computationally efficient, its non-spatial nature ignores the territorial dependence structure of bathymetry. To overcome this limitation, Kriging with External Drift (*KED*) was implemented, a geostatistical method that integrates the Sentinel-2 optical predictor with the spatial continuity of the seabed (Chiles and Delfiner 2012; Goovaerts 2000).

KED combines a deterministic drift component $\widehat{d}(s)$, derived from the stratified optical model, with a residual $\widehat{e}(s)$ interpolated using ordinary kriging (Casal et al. 2019):

$$Z_{KED}(s) = \widehat{d}(s) + \widehat{e}(s) \quad (4)$$

The drift captures the linear relationship between depth and *SDB* signal, derived from the logarithmic ratio of Sentinel-2 bands B2 and B3, inheriting the physical assumptions of Stumpf et al. (2003) on optical penetration in clear waters. The residual component models the variability not explained by the optical signal, using a variogram to describe the spatial autocorrelation of bathymetric deviations. The sequential estimation of the two components, first the drift, then the residuals, ensures computational stability over large spatial domains such as lagoons (Casal et al. 2019). The drift was calibrated by implementing Stumpf's model on a subset of 10,000 points, adopting stratified calibration by substrate type (sand vs. mud) as described in the previous section. This approach generated a drift sensitive to variations in benthos reflectance, reducing the amount of residuals assigned to the geostatistical component.

Once the deterministic basis was defined, the point residuals were calculated as:

$$e(s_i) = Z_{CNR}(s_i) - \widehat{d}(s_i) \quad (5)$$

where $Z_{\mathrm{CNR}}(s_i)$ is the measured depth and $\widehat{d}(s_i)$ is the radiometric estimate. Analysis of these residuals confirmed the absence of systematic distortions, with a random error centred around zero.

Variographic analysis was conducted on a sample of 5,000 points randomly extracted from the residual dataset. The results highlighted a structured spatial dependence of the error: the fitting of a spherical model yielded a range of 1201.50 m, indicating that the discrepancies in the optical model maintain spatial correlation for over a kilometre. The nugget effect, which quantifies the unstructured variance attributable to measurement errors or spatial variability

Table 6 Calibration parameters and accuracy metrics of the SDB model for depth classes

Bathymetric class	Angular coefficient (m1)	Intercept (m0)	R^2	RMSE (m)	Bias (m)	MAE (m)	Points
Global model	-15.54	103.38	0.87	1.09	-0.41	0.59	2310
0 / -1 m (Class 1)	-0.00237	-1.07	0.155	0.49	-0.43	0.42	924
-1 / -2 m (Class 2)	-0.00149	-1.54	0.095	0.33	-0.16	0.28	940
-2 / -4 m (Class 3)	-0.00168	-2.99	0.031	0.67	-0.36	0.60	196
-4 / -6 m (Class 4)	0.00452	-4.21	0.021	0.95	+0.75	0.76	88
-6 / -18 m (Class 5)	-0.0536	-12.00	0.119	3.74	-2.49	3.23	162

at a scale smaller than the sampling distance (Chiles and Delfiner 2012) is negligible: this indicates that the residuals do not exhibit discontinuities at the local scale and that their spatial structure is reliably described by the spherical model alone, allowing kriging to interpolate continuously over the entire domain. Once the spatial structure of the error was confirmed, the deterministic component was calculated for each pixel of the Sentinel-2 images and then corrected by the continuous surface of the residuals generated by kriging. The implementation was optimised using a tiling strategy (250 × 250 pixel blocks) and a local search limited to the 32 nearest points per pixel (a neighbourhood size selected to balance statistical reliability and computational efficiency) implementing a local kriging approach in which each prediction relies solely on spatially proximate observations. At the end of the global generation, a reliability mask was applied to exclude physically implausible values, with a clamping range set between +1.5 m and −60.0 m. This extended threshold was chosen to preserve the morphological integrity of the deepest navigable channels, where the integration of the residuals allowed bathymetric information to be recovered beyond the limits of optical penetration alone.

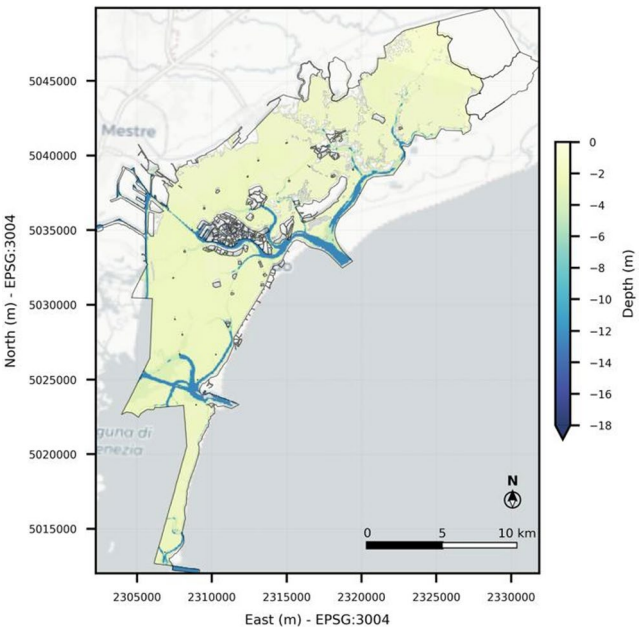


Fig. 2 Basin-scale bathymetric reconstruction of the Venice Lagoon obtained using the log-ratio model of Stumpf et al. (2003) with stratified calibration by depth classes (GT: 2002 dataset)

Results

Axis I: *SDB* modelling and stratified validation by comparison with the 2002 dataset

The analysis of stratified linear regressions by bathymetric classes (Table 6) shows significant variability in the strength of the link between pseudo-bathymetry (*pSDB*) and actual depth. The performance shows a significant technical challenge in the deepest classes: the −6 / -18 m range has a coefficient of determination (R^2) of 0.119, with an RMSE rising to 3.74 m, reflecting the physiological extinction of the optical signal as the water column increases. In contrast, the surface and intermediate classes show very low absolute errors: the −1/-2 m range (Class 2) has an RMSE of 0.33 m, while the −2/-4 m range (Class 3) has a value of 0.67 m. The low values of the R^2 s found within the individual classes are attributable to the reduced range of depth variation considered (narrow range) and to the micro-variability of the seabed, which acts as background noise on the spectral response. This signal stability in shallow water areas is confirmed by the metric accuracy, despite local turbidity phenomena that can fragment the linearity of the pSDB.

A determining factor for the statistical robustness of the model is the distribution of the sample size. The data show that the most superficial classes are heavily represented (Classes 1 and 2 have 924 and 940 samples each, respectively), while the deeper classes are significantly less populated (r Class 4 drops to 88 control points). This unevenness, combined with natural light attenuation, explains the greater uncertainty found in the channels. The integration of these segmented models has allowed the generation of a continuous bathymetric raster (Fig. 2) in which the range of values obtained is consistent with the expected morphology in the lagoon domain, clearly distinguishing the main channels from the shallow mudflats.

Statistical validation conducted through direct comparison with the reference raster over the entire domain reveals an average error (bias) of -0.41 m, which indicates a

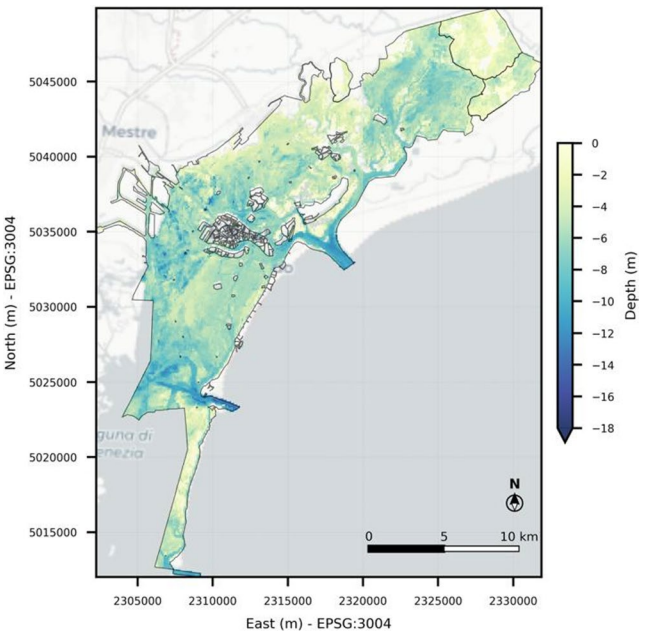


Fig. 3 Basin-scale bathymetric reconstruction of the Venice Lagoon obtained using the log-ratio model of Stumpf et al. (2003) with single global calibration without stratification (GT: 2013 dataset)

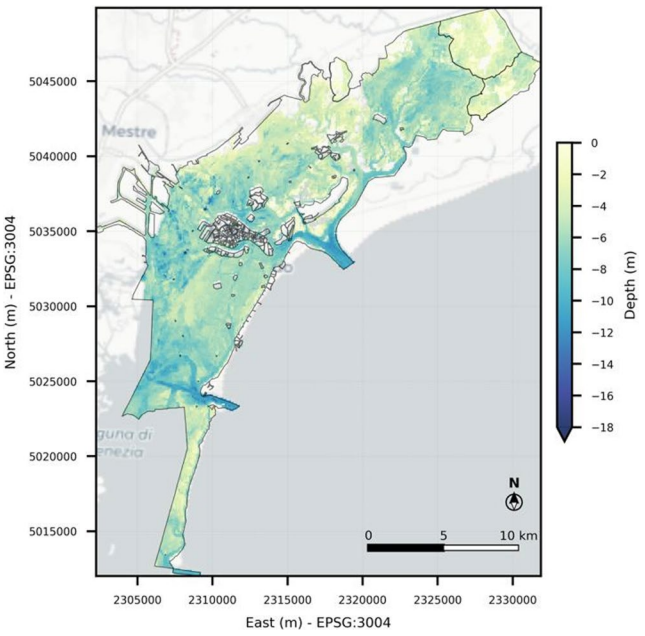


Fig. 4 Basin-scale bathymetric reconstruction of the Venice Lagoon obtained using the log-ratio model of Stumpf et al. (2003) with stratified calibration by substrate type (Sand vs. Mud) (GT: 2013 dataset)

tendency for the model to slightly underestimate depths. The RMSE value calculated over the entire domain is 1.09 m: a result that confirms good overall adherence between estimated and observed data, with an acceptable level of dispersion for territorial-scale monitoring applications. The analysis was completed with the construction of a global regression model based on a robust sample of 2310 points. This processing returned a global R^2 of 0.87, documenting the high capacity of the Sentinel-2 sensor to respond to the complex bathymetric gradients of the Venice Lagoon when considering the entire altimetric range.

Axis 2: Substrate characterisation and *SDB-KED* integration and stratified validation through comparison with the CNR-ISMAR 2013 dataset

The implementation of the methodology in Axis 2 initially involved the calibration of Stumpf's log-ratio model over the entire lagoon domain (Fig. 3).

The results of the global calibration (Table 7) highlight the intrinsic limitations of a purely radiometric approach in an optically complex environment such as the Venice Lagoon.

From an analytical perspective, an RMSE of 4.02 m and an R^2 of 0.20 suggest that the single global regression is unable to effectively discriminate between exogenous variables, such as variable turbidity and different benthos reflectance. The bias value (-0.46 m) indicates a general tendency of the model to underestimate actual depths.

In order to refine the estimate, stratification based on substrate type was introduced, differentiating the parameters for the macro-categories of seabed: Sand and Mud (Fig. 4). The hypothesis underlying this step s that the spectral response of *the pSDB* was significantly influenced by the differentiated reflectance of the sediments.

However, as reported in Table 8, segmentation by substrate did not produce a substantial improvement in global

Table 7 Calibration parameters and accuracy metrics of Stumpf's global SDB model

Bathymetric class	Angular coefficient (m1)	Intercept (m0)	R^2	RMSE (m)	Bias (m)	MAE (m)	Points
Global model	-160.61	149.06	0.20	4.02	-0.46	3.38	814

Table 8 Calibration parameters and accuracy metrics of Stumpf's global SDB model stratified by substrate

Category	Angular coefficient (m1)	Intercept (m0)	R^2	Root mean square error (m)	Bias (m)	MAE (m)	Points (*n*)
Sand	-103.08	92.99	0.26	5.14	+0.50	3.85	49
Mud	-153.83	142.41	0.23	4.39	-0.53	3.34	385
Global (Strat.)	N/A	N/A	0.17	4.07	-0.35	3.40	434

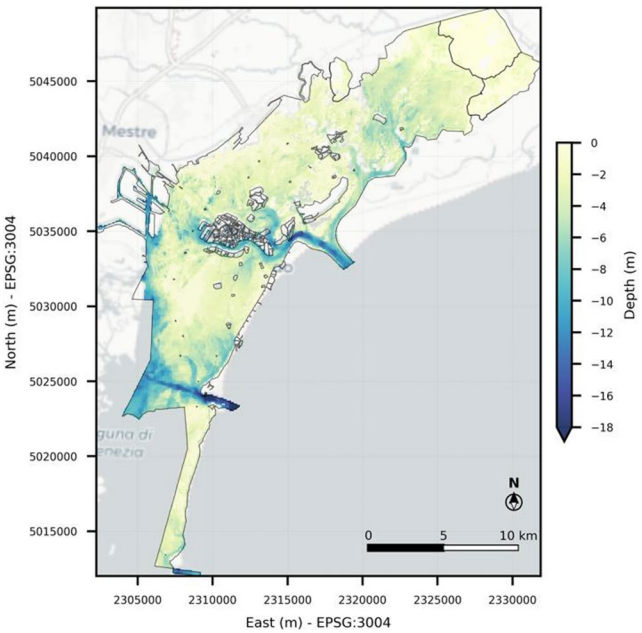


Fig. 5 Basin-scale bathymetric reconstruction of the Venice Lagoon obtained by integrating the log-ratio model of Stumpf et al. (2003) stratified by substrate with Kriging with External Drift (*SDB-KED*) (GT: 2013 dataset)

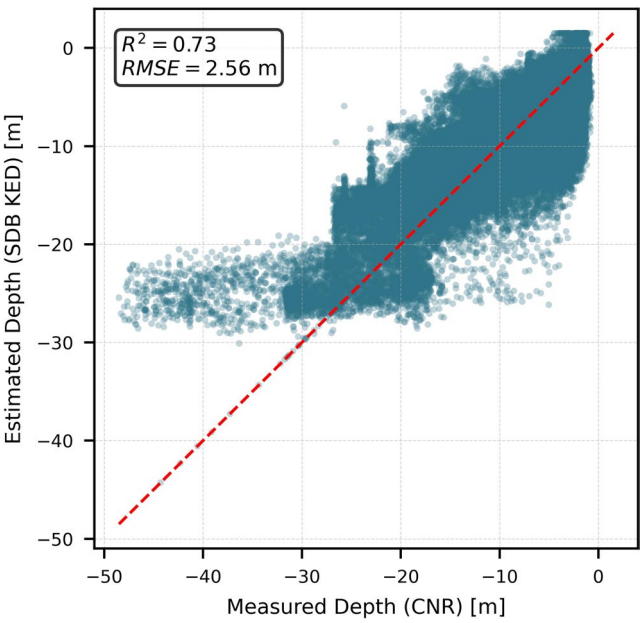


Fig. 6 Validation scatterplot of the *SDB-KED* model

Table 9 Calibration parameters and accuracy metrics of Stumpf's global SDB model stratified by substrate with KED

Bathymetric class	R^2	RMSE (m)	Bias (m)	MAE (m)	Points
Global model	0.730	2.556	-0.093	1.819	320 231

metrics, but rather showed a slight increase in the overall mean square error.

Detailed analysis shows that the Sand class, despite having a slightly higher R^2 (0.26), has the highest error (RMSE 5.14 m), probably due to the location of these deposits in areas subject to intense hydro-morphological dynamics (such as harbour mouths or major canals) where the saturation of the optical signal is more pronounced. The Mud class, which represents most of the lagoon domain, shows an RMSE of 4.39 m.

These results confirm that, although the nature of the seabed influences the spectral signature, it is not the only limiting factor. The persistence of a high RMSE in both models (global and stratified) demonstrates that the radiometric component alone is not sufficient for an accurate bathymetric reconstruction of the entire Venetian basin, making it necessary to integrate spatial correction techniques and use advanced geostatistical models to mitigate residual uncertainty.

In line with the analysis of the optical component, spatial integration obtained through Kriging with External Drift (*KED*) marked an interesting methodological advance. This hybrid approach made it possible to overcome the physical barriers of radiometry alone, using the stratified *SDB* map as an external trend (drift) and locally correcting deviations through the interpolation of residuals calculated on the extensive CNR-ISMAR 2013 ground truth dataset (Fig. 5).

The results from the final model, shown in Table 9, show an increase in performance: the coefficient of determination (R^2) rises to 0.730, indicating that the model is now able to explain almost three quarters of the complex bathymetric variability of the entire lagoon basin.

From a statistical point of view, the reduction of the bias to a value close to zero (-0.093 m) demonstrates the substantial removal of the systematic underestimation that plagued previous attempts. Although the absolute value of the RMSE is 2.55 m, this figure should not be interpreted as a deterioration in quality, but rather as a reflection of a model that is now capable of operating over the entire depth range, including the deepest channels that were invisible in pure optical models due to signal saturation. The effectiveness of this synergy between geostatistics and remote sensing is confirmed by the validation scatterplot (Fig. 6).

Analysis of the scatter plot reveals a marked adherence to the line of perfect correspondence (1:1), especially in the range between zero and −15 m, where the density of points is highest and the dispersion is minimal. In this range, the optical component provides a solid morphological basis that the *KED* refines with extreme precision. Moving towards higher bathymetries, between −15 and −30 m, there is greater lateral dispersion due to the extinction of light in the water. However, the model does not lose the real trend and continues to follow the seabed pattern thanks to the spatial

correction of the residuals. The compactness of the point cloud and the low MAE value confirm that the *SDB-KED* integration has succeeded in normalising the anomalies related to turbidity and the nature of the substrate, returning a bathymetric reconstruction with good resolution that is morphologically consistent and statistically reliable for the entire domain of the Venice Lagoon.

In order to understand any geographical patterns of error, a map of the spatial distribution of the residuals was produced. Figure 7 shows the distribution of errors over the lagoon basin.

Analysis of the residual map reveals that areas characterised by shallows and tidal flats have minimal deviations, with values mainly ranging between +/- 1 m, confirming the high reliability of the model in morphologically stable areas. The most marked fluctuations are observed at the slopes of the major canals and harbour mouths: in these areas, the residuals tend to increase due to the steep slopes of the seabed, where even a minimal spatial shift between the sample data and the satellite pixel can generate more noticeable metric deviations.

Despite the presence of localised extreme values, attributable to areas with very active sedimentary dynamics or instrumental limitations in the deepest bathymetry, the prevalence of neutral tones in the map confirms the effectiveness and of the model tested to correct the original radiometric distortions. From an analytical point of view, the spatial distribution highlights some critical issues located near the coastline and the mainland, where the appearance of more intense colour tones (red areas) suggests the persistence of uncertainties related to complex refraction phenomena or the high concentration of suspended sediments: these variables introduce background noise that the *KED* algorithm was unable to completely neutralise. At the same time, the observation of uniform colouring in the open sea sectors is symptomatic of the light penetration limit being reached, confirming the existence of a bathymetric horizon beyond which the optical signal decays (a phenomenon that can be seen in the 'floor' highlighted in the scatterplot at greater depths). Finally, the sporadic presence of pixels with very saturated colours but geographically isolated should be interpreted as the manifestation of point outliers, attributable to potential systematic errors or artefacts present in the original ground truth data, rather than to an inefficiency of the estimation model.

The robustness of the *KED* model is further confirmed by the histogram analysis of the probability density of residual errors. The frequency distribution is strongly centred on zero (Fig. 8), with a trend indicating a marked concentration of deviations in a very narrow range around the mean value. A comparison between the actual distribution of residuals and the theoretical Gaussian curve shows that the model is

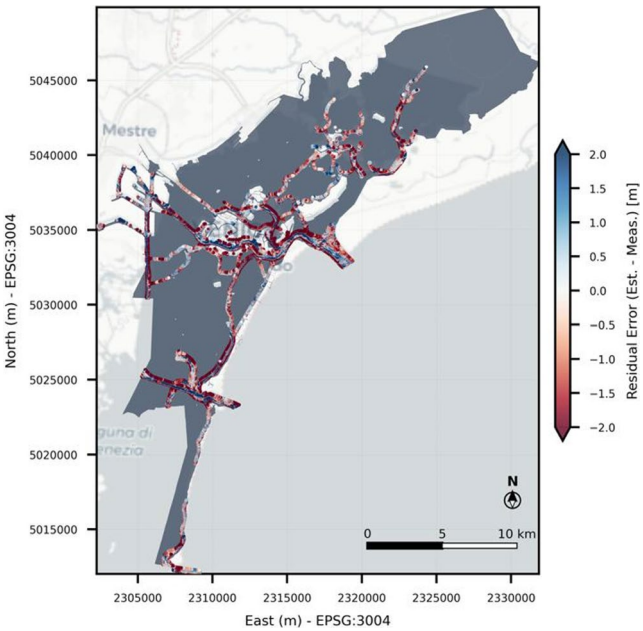


Fig. 7 Spatial distribution of *SDB-KED* model residuals

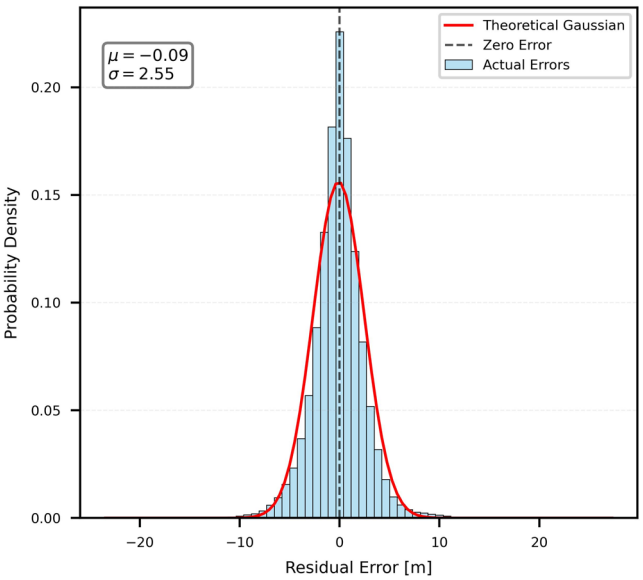


Fig. 8 Analysis of the distribution of residual errors in the *SDB-KED* model

more accurate than a purely random distribution: the density of errors close to zero is significantly higher than the theoretical curve, indicating effective calibration over most of the lagoon basin.

The average error value (μ = -0.09 m), which almost coincides with the "Zero Error" line, confirms the absence of significant systematic drifts, guaranteeing the impartiality of the bathymetric estimates produced. Although the standard deviation (σ = 2.55 m) is affected by the dispersion produced by areas of high depth and the aforementioned

channel slopes, the symmetry of the bell curve shows that overestimation and underestimation errors are almost perfectly balanced. This statistical behaviour, combined with adherence to normal distribution, confirms that the proposed hybrid methodology has succeeded in transforming the initial radiometric noise into a coherent bathymetric signal, whose residual uncertainties are random in nature and spatially limited to the most morphologically complex contexts of the lagoon.

To complete the statistical validation, a disaggregated error analysis was conducted to assess the sensitivity of the model to variations in the water column. Although the overall analysis of the residuals confirms the impartiality of the model, the physical nature of the satellite signal requires consideration of the loss of predictive capacity induced by radiative extinction. Figure 9 graphically illustrates the decay in accuracy (expressed in terms of RMSE) across different bathymetric ranges.

From an analytical point of view, the results show excellent performance within the first 5 metres of depth, where the RMSE remains low, ranging between 1.80 m and 2.20 m. In this range, the penetration of visible light (particularly in the blue and green bands) ensures an optimal signal-to-noise ratio, allowing the *drift* component of the *KED* model to operate on an extremely solid morphological basis. The statistical robustness of these bands is guaranteed by an extremely high sample size, with 13,271 samples in the 0–2 m range and a peak of 67,572 units in the 2–4 m band, followed by 66,340 points in the 4–6 m range. In these areas, which include almost all of the tidal flats and lagoon shallows, the contribution of remote sensing is predominant and geostatistical correction is only used to refine local details. Above the −10 metre threshold, there is a progressive and marked increase in uncertainty. In the deepest areas, the RMSE tends to stabilise at values above 4.50 m, reaching maximum peaks in the large navigation channels and areas near the harbour mouths (beyond −15 metres). This phenomenon of 'accuracy decay' is attributable to the saturation of the optical signal: the energy reflected from the bottom becomes indistinguishable from the noise caused by atmospheric *scattering* and water turbidity. Although the density of control points undergoes a physiological reduction in the higher depth classes, with 15,089 samples between 15 and 20 m and 5,968 samples between 20 and 35 m, the dataset remains sufficiently large to confirm the trend of increasing error. The deterministic component of the model (*SDB*) loses its effectiveness in such contexts, delegating the entire bathymetric reconstruction to the stochastic component of *the KED* (residual interpolation). The proposed integrated approach demonstrates an operational duality: it is configured as a precision tool for monitoring surface morphological systems, while it takes on an indicative morphological

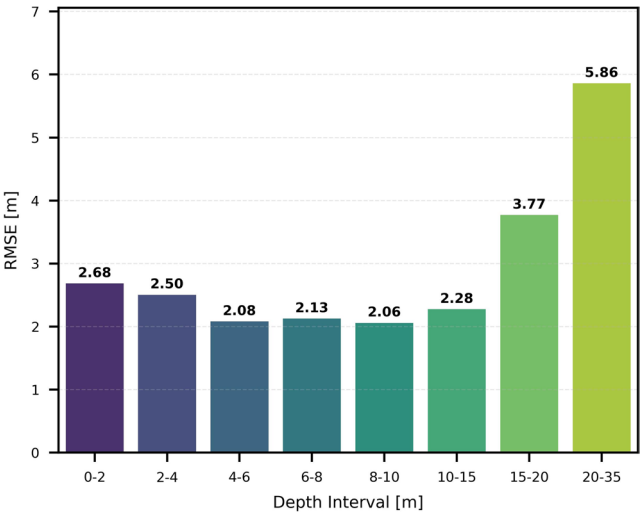


Fig. 9 RMSE values broken down by depth class

estimation function for large lagoon arteries. This distinction is fundamental for defining the domains of applicability of the model produced, confirming that the integration of Sentinel-2 data and geostatistical techniques represents a solution for mapping coastal and lagoon environments, while remaining bound by the physical limitations imposed by underwater optics (Tassetti et al. 2025; Maltese et al. 2024).

Discussions

This work, tested in the Venice Lagoon, has outlined a performance framework for *SDB* in complex environments. A crucial strength of the methodology lies in its high replicability: the exclusive use of open source data (Sentinel-2) and cloud computing platforms makes this approach easily replicable in other contexts with similar characteristics. The results obtained confirm that, although the Sentinel-2 sensor has the spectral resolution necessary to identify bathymetric gradients, the accuracy of the estimate remains conditioned by environmental variables that act as non-linear disturbance factors.

The evidence emerging from Axis I indicates that the spectral resolution of the sensor, although theoretically adequate, is not sufficient to compensate for the influence of local forcing factors. Specific environmental factors in the lagoon domain act as disturbance elements, altering the linearity of the relationship between optical signal and depth. The variability found in the coefficients of determination between the different bathymetric depth classes highlights that depth is not the only factor governing the reflectance recorded by the sensor. The significant drop in performance in the intermediate ranges (-2 /-4 m) shows an 'optical

saturation zone' where the spectral signature of the seabed is gradually cancelled out by the contributions of the water volume. In these areas, the high concentration of suspended solids (TSS) and chlorophyll, easily found in a lagoon environment, induces scattering phenomena that lead to a systematic overestimation of the seabed (evidenced by *the* negative *bias* of -0.421 m).

Contrary to expectations, the greater predictive capacity observed in the deep classes (-6 /-18 m) should not be interpreted as superior signal penetration, but rather as a response to morphologically more stable and optically more homogeneous seabeds. However, as emerged from the analysis of the sample size, the small number of control points in these ranges calls for caution, suggesting the risk of statistical *overfitting* that may not reflect the true accuracy of the model. The extension of the analysis in Axis 2 mitigated this risk through the use of an extremely robust independent validation dataset (CNR-ISMAR 2013), consisting of over 320 000 points.

In addition to these aspects, there is the limitation related to the time window of the analysis in Axis 1, which was too small for the specificities of the site. To overcome this critical issue, Axis 2 adopted a broader time selection (March-June 2020), allowing the generation of a multi-temporal composite based on the 25th percentile of reflectance. This strategy made it possible to effectively mediate transient fluctuations in turbidity and tidal cycles, isolating the conditions of maximum transparency of the water column.

The comparison between Stumpf's global approach and the stratified variant developed in Axis 2 allows us to take stock of the real predictive capabilities of remote sensing in complex contexts. Although substrate stratification represents a conceptual advance, quantitative analysis reveals performance conditioned by the nature of the benthos. The most immediate evidence is the flattening of the global model on the dominant class (Mud): the regression parameters of the global model are almost superimposable on those of mud, making the global calibration effectively 'blind' with respect to sandy areas. The introduction of a seabed classification using Random Forest has made it possible to isolate specific slopes for sand and mud. Although the background noise related to turbidity persists, differentiated calibration has improved the spatial consistency of the data, correcting for systematic ' ' biases related to the different reflectance of sediments. However, residual analysis confirmed that a significant portion of the variance (over 80% in some critical areas) cannot be explained by the purely deterministic optical model alone.

It is in this scenario that the value of *SDB-KED* integration comes into play. Variographic analysis has shown that the *SDB* model error is not random but has a clear spatial autocorrelation structure. The use of Kriging with External Drift has radically transformed the role of the satellite: *SDB* bathymetry is no longer the final product, often affected by metric uncertainties that are unacceptable for consultation and use, but acts as an 'external drift' that guides the interpolation of direct surveys. This hybrid approach has made it possible to 'anchor' the satellite estimate to the centimetre accuracy of in-situ surveys, propagating this accuracy even in optically critical areas (channels up to -15/-18 m deep) or areas not accessible to recent surveys. The final result is a bathymetric dataset with a resolution of 10 m that combines the areal coverage of remote sensing with the analytical rigour of geostatistical models. This integration has made it possible to test a new methodological tool for monitoring transition areas, providing cartographic output suitable for supporting maritime space management and planning strategies in dynamic environmental contexts.

Conclusions

This study investigated the potential and critical issues of Satellite Derived Bathymetry (*SDB*) in a morphologically and optically complex environment such as the Venice Lagoon. The methodological approach, structured around two lines of research, made it possible to test a hybrid protocol capable of combining the spatial continuity offered by remote sensing with the metric precision of in situ surveys, focusing on a coherent morphological reconstruction. The work confirmed that the data acquired by the Sentinel-2 constellation has a spectral resolution suitable for intercepting bathymetric gradients, offering a synchronous, systematic and freely accessible overview. However, it has become clear that reflectance alone is an unstable indicator in the presence of 'environmental noise', understood as variable turbidity, signal saturation and benthos interference, making purely radiometric models insufficient for high-precision hydrographic purposes (Misra et al. 2018).

The integration of the *SDB* model with Kriging with External Drift represents the main methodological contribution of the work. This geostatistical approach has made it possible to mitigate the intrinsic disturbances of the optical signal, treating the satellite data not as a definitive output, but as an auxiliary variable (drift) for the interpolation of in situ measurements. This synergy has facilitated the generation of a continuous bathymetric surface ( ), characterised by solid metric consistency and high fidelity in morphological reconstruction. The *SDB-KED* combination has proven to be the best-performing model, ensuring an optimal balance between the spatial resolution of remote data and the accuracy of direct surveys.

The use of open source data and cloud computing platforms (Google Earth Engine and Google Colab) ensures that

the proposed protocol is highly replicable in other contexts with similar physical characteristics.

Alongside these results, it is necessary to explicitly recognise the limitations imposed by the native spatial resolution of the Sentinel-2 sensor, which is 10 m for the optical bands used. Although this granularity is adequate for characterising tidal flats and main channels, it is insufficient to accurately reproduce the morphology of sub-pixel elements such as minor ghebi, secondary channel slopes and sandbar-mudflat transitions. In these contexts, the radiometric response of each pixel integrates contributions from heterogeneous environments, emerged surfaces, shallow waters and vegetation, introducing a spectral mixing effect that degrades the quality of the local bathymetric estimate. The result is a tendency towards morphological smoothing, with underestimation of depths in narrower channels and overestimation in transition areas, an effect that the geostatistical component of *KED* can only partially mitigate in the absence of densely distributed control points. Future applications of the protocol could benefit from integration with high spatial resolution sensors, such as WorldView-2/3, PlanetScope or data acquired from UAV platforms (Agrafiotis et al. 2019; Karaki et al. 2022), which would extend the validity of bathymetric estimation to morphological scales not previously accessible to passive satellite remote sensing.

The results obtained make this contribution a first step in a broader process of increasing knowledge of the vertical dimension in territorial and maritime planning processes.

The work proposes a replicable and scalable methodological framework, geared towards the progressive construction of dynamic and multi-temporal monitoring systems. Such systems are essential to support informed decision-making processes, capable of integrating the morphological and volumetric components of coastal systems into coastal spatial planning and maritime space management tools.

The approach outlined therefore contributes to the construction of a structured knowledge base capable of feeding adaptive governance processes in land-sea transition areas.

Author contributions All authors contributed to the study conception and design. Material preparation, data collection, and GIS analysis were performed by the first author. The first draft of the manuscript was written by the first author. The second author provided supervision and performed critical revision of the manuscript for important intellectual content. All authors commented on previous versions of the manuscript, read, and approved the final version.

Funding Open access funding provided by Università degli Studi di Roma La Sapienza within the CRUI-CARE Agreement. Not applicable.

Data availability The datasets generated during and/or analysed during the current study are available from the corresponding author on reasonable request.

Declarations

Competing interests The authors have no relevant financial interests to disclose. C. Balletti is one of the Guest Editors of the Special Issue "Geomatics in a Changing World" in Applied Geomatics, to which this manuscript is submitted. She has declared this competing interest and will be excluded from all editorial decisions regarding this submission, which will be handled by one of the other Guest Editors.

Open Access This article is licensed under a Creative Commons Attribution 4.0 International License, which permits use, sharing, adaptation, distribution and reproduction in any medium or format, as long as you give appropriate credit to the original author(s) and the source, provide a link to the Creative Commons licence, and indicate if changes were made. The images or other third party material in this article are included in the article's Creative Commons licence, unless indicated otherwise in a credit line to the material. If material is not included in the article's Creative Commons licence and your intended use is not permitted by statutory regulation or exceeds the permitted use, you will need to obtain permission directly from the copyright holder. To view a copy of this licence, visit http://creativecommons.org/licenses/by/4.0/.

References

Agrafiotis P, Skarlatos D, Georgopoulos A, Karantzalos K (2019) Shallow water bathymetry mapping from UAV imagery based on machine learning. arXiv preprint arXiv:1902.10733

Ahola R, Chénier R, Sagram M, Horner B (2020) The impact of sensors for satellite derived bathymetry within the Canadian Arctic. Geomatica 74(2):46–64

Ashphaq M, Srivastava PK, Mitra D (2021) Review of near-shore satellite derived bathymetry: classification and account of five decades of coastal bathymetry research. J Ocean Eng Sci 6(4):340–359

Caballero I, Stumpf RP (2019) Retrieval of nearshore bathymetry from Sentinel-2A and 2B satellites in South Florida coastal waters. Estuar Coast Shelf Sci 226:106277

Campa S (2007) Environmental problems in Mediterranean cities: the cases of Venice and Sete. Dissertation, University of Bologna

Casal G, Monteys X, Hedley J, Harris P, Cahalane C, McCarthy T (2019) Assessment of empirical algorithms for bathymetry extraction using Sentinel-2 data. Int J Remote Sens 40(8):2855–2879

Casal G, Harris P, Monteys X, Hedley J, Cahalane C, McCarthy T (2020) Understanding satellite-derived bathymetry using Sentinel 2 imagery and spatial prediction models. GIScience Remote Sens 57(3):271–286

Chiles JP, Delfiner P (2012) Geostatistics: modelling spatial uncertainty, 2nd edn. Wiley, New York

Creamer C, O'Hagan AM, Ritchie H, De Sutter R (2020) How can MSP support resilience of European land sea interactions. ESPON Topic Paper. European Spatial Planning Observation Network, Luxembourg

D'Alpaos A (2011) The mutual influence of biotic and abiotic components on the long-term ecomorphodynamic evolution of salt-marsh ecosystems. Geomorphology 126(3–4):269–278

Del Savio AA, Luna Torres A, Vergara Olivera MA, Llimpe Rojas SR, Urday Ibarra GT, Neckel A (2023) Using UAVs and photogrammetry in bathymetric surveys in shallow waters. Appl Sci 13(6):3420

Elliott M, Burdon D, Hemingway KL, Apitz SE (2007) Estuarine, coastal and marine ecosystem restoration: confusing management and science—a revision of concepts. Estuar Coast Shelf Sci 74(3):349–366

European Commission (2014) Directive 2014/89/EU of the European Parliament and of the Council of 23 July 2014 establishing a framework for maritime spatial planning. Off J Eur Union L 257:135–145

Fernandez-Diaz JC, Glennie CL, Carter WE, Shrestha RL, Sartori MP, Singhania A et al (2013) Early results of simultaneous terrain and shallow water bathymetry mapping using a single-wavelength airborne LiDAR sensor. IEEE J Sel Top Appl Earth Obs Remote Sens 7(2):623–635

Ferrando I, Brandolini P, Federici B, Lucarelli A, Sguerso D, Morelli D, Corradi N (2021) Coastal modification in relation to sea storm effects: Application of 3D remote sensing survey in Sanremo Marina (Liguria, NW Italy). Water 13(8):1040

Ferreira IO, Andrade LCD, Teixeira VG, Santos FCM (2022) State of the art of bathymetric surveys. Bol Ciênc Geod 28:e2022002

Feyisa GL, Meilby H, Fensholt R, Proud SR (2014) Automated Water Extraction Index: A new technique for surface water mapping using Landsat imagery. Remote Sens Environ 140:23–35

Figliomeni FG, Parente C (2023) Bathymetry from satellite images: A proposal for adapting the band ratio approach to IKONOS data. Appl Geomat 15(3):565–581

Francis H, Traykovski P (2021) Development of a highly portable unmanned surface vehicle for surf zone bathymetric surveying. J Coast Res 37(5):933–945

Gao J (2009) Bathymetric mapping by means of remote sensing: methods, accuracy and limitations. Prog Phys Geogr 33(1):103–116

Gatto P, Carbognin LTHE (1981) The Lagoon of Venice: natural environmental trend and man-induced modification. Hydrol Sci J 26(4):379–391

Gianinetto M, Lechi G (2004) Use of high-resolution multispectral data for monitoring the Venice lagoon. The use of high-resolution satellite images for territorial analysis. AIT, ASITA, SIFET, pp 119–134

Goovaerts P (1997) Geostatistics for natural resources evaluation. Oxford University Press, New York

Goovaerts P (2000) Geostatistical approaches for incorporating elevation into the spatial interpolation of rainfall. J Hydrol 228(1–2):113–129

Hedley JD, Harborne AR, Mumby PJ (2005) Simple and robust removal of sun glint for mapping shallow-water benthos. Int J Remote Sens 26(10):2107–2112

Hedley J, Roelfsema C, Koetz B, Phinn S (2012) Capability of the Sentinel 2 mission for tropical coral reef mapping and coral bleaching detection. Remote Sens Environ 120:145–155

Hodúl M, Bird S, Knudby A, Chénier R (2018) Satellite derived photogrammetric bathymetry. ISPRS J Photogramm Remote Sens 142:268–277

Iglesias-Campos A, Rubeck J, Sanmiguel-Esteban D, Schwarz G (2021) MSPglobal International Guide on Marine/Maritime Spatial Planning. UNESCO

Innocenti A, Musco F (2023) Land-sea interactions: A spatial planning perspective. Sustainability 15(12):9446

IPCC (2022) Climate change 2022: impacts, adaptation and vulnerability. Contribution of Working Group II to the Sixth Assessment Report of the Intergovernmental Panel on Climate Change. Cambridge University Press, Cambridge

ISPRA (2023) Climate indicators in Italy in 2022. State of the Environment No. 104/23. ISPRA, Rome

Kader A, Chowdhury MZR, Uddin MM, Hoque ME, Basak SC (2013) Bathymetric study of the Bay of Bengal based on open source satellite and sounding data. Int J Geomat Geosci 4(1):116

Karaki AA, Bibuli M, Caccia M, Ferrando I, Gagliolo S, Odetti A, Sguerso D (2022) Multi-platform and multi-sensor integrated survey for submerged and emerged areas. J Mar Sci Eng 10(6):753

Lurton X, Lamarche G, Brown C, Lucieer V, Rice G, Schimel A, Weber T (2015) Backscatter measurements by seafloor-mapping sonars: guidelines and recommendations. GEOHAB Report, p 200

Lyzenga DR (1978) Passive remote sensing techniques for mapping water depth and bottom features. Appl Opt 17(3):379–383

Lyzenga DR, Malinas NP, Tanis FJ (2006) Multispectral bathymetry using a simple physically based algorithm. IEEE Trans Geosci Remote Sens 44(8):2251–2259

Madricardo F, Foglini F, Trincardi F (2017a) Processed high-resolution ASCII: ESRI gridded bathymetry data (EM2040 and EM3002) from the Lagoon of Venice collected in 2013. Interdisciplinary Earth Data Alliance (IEDA)

Madricardo F, Foglini F, Kruss A, Ferrarin C, Pizzeghello NM, Murri C, Trincardi F (2017b) High resolution multibeam and hydrodynamic datasets of tidal channels and inlets of the Venice Lagoon. Sci Data 4:170042

Mahrad BE, Newton A, Icely JD, Kacimi I, Abalansa S, Snoussi M (2020) Contribution of remote sensing technologies to a holistic coastal and marine environmental management framework: a review. Remote Sens 12(14):2313

Maltese A, Presti VL, Nocera GA, Sulli A (2024) Comparison of bathymetry estimated from multibeam echosounder and optical data. Remote Sensing for Agriculture, Ecosystems, and Hydrology XXVI, vol 13191. SPIE, pp 26–32

McFeeters SK (1996) The use of the Normalised Difference Water Index (NDWI) in the delineation of open water features. Int J Remote Sens 17(7):1425–1432

Misra A, Vojinovic Z, Ramakrishnan B, Luijendijk A, Ranasinghe R (2018) Shallow water bathymetry mapping using Support Vector Machine (SVM) technique and multispectral imagery. Int J Remote Sens 39(13):4431–4450

Monteys X, Harris P, Caloca S, Cahalane C (2015) Spatial prediction of coastal bathymetry based on multispectral satellite imagery and multibeam data. Remote Sens 7(10):13782–13806

O'Hagan AM, Paterson S, Le Tissier M (2020) Addressing the tangled web of governance mechanisms for land-sea interactions: Assessing implementation challenges across scales. Mar Policy 112:103715

Ravera O (2000) The Lagoon of Venice: the result of both natural factors and human influence. J Limnol 59(1):19–30

Sarretta A, Pillon S, Molinaroli E, Guerzoni S, Fontolan G (2010) Sediment budget in the Lagoon of Venice, Italy. Cont Shelf Res 30:934–949. https://doi.org/10.1016/j.csr.2009.07.002

Schlüter A, Van Assche K, Hornidge AK, Văidianu N (2020) Land-sea interactions and coastal development: An evolutionary governance perspective. Mar Policy 112:103801

Stumpf RP, Holderied K, Sinclair M (2003) Determination of water depth with high-resolution satellite imagery over variable bottom types. Limnol Oceanogr 48(1part2):547–556

Tagliapietra D, Magni P, Basset A, Viaroli P (2014) Coastal transition ecosystems: recent transformations, direct anthropogenic pressures and possible impacts of climate change. Biol Ambient 28(2):101–111

Tassetti AN, Simone G, Avanzato G, Malinverni ES, Memmola F, Brocchini M, Penna P (2025) Integrated geomatics for seamless coastal mapping: a vulnerable coastline in the central Adriatic Sea. Geomat Nat Hazards Risk 16(1):2584699

Torelli G (2020) Combating climate change in land management. A PAESC for the Venice lagoon. Federalismi.it

Toso C (2017) Recent morphological-sedimentary evolution of the Lido port mouth (Venice Lagoon-Italy). Dissertation, Ca' Foscari University of Venice

Xu H (2006) Modification of normalised difference water index (NDWI) to enhance open water features in remotely sensed imagery. Int J Remote Sens 27(14):3025–3033

Xu T, Liu Y, Tang L, Liu C (2022) Improvement of Kriging interpolation with learning kernel in environmental variables study. Int J Prod Res 60(4):1284–1297

Publisher's note Springer Nature remains neutral with regard to jurisdictional claims in published maps and institutional affiliations.